Anisotropic spin fluctuations and anomalies of nuclear quadrupole interactions in the itinerant antiferromagnet $NpCoGa_5$: ^{59}Co NMR and $^{69,71}Ga$ NMR/NQR studies

Hironori Sakai,[1] Shinsaku Kambe,[1] Yo Tokunaga,[1] Tatsuya Fujimoto,[1] Russell E. Walstedt,[1,*] Hiroshi Yasuoka,[1] Dai Aoki,[2,†] Yoshiya Homma,[2] Etsuji Yamamoto,[1] Akio Nakamura,[1] Yoshinobu Shiokawa,[1,2] and Yoshichika Ōnuki[1,3]

[1]*Advanced Science Research Center, Japan Atomic Energy Agency, Tokai, Naka, Ibaraki 319-1195, Japan*

[2]*Institute for Materials Research, Tohoku University, Oarai, Ibaraki 311-1313, Japan*

[3]*Graduate School of Science, Osaka University, Toyonaka, Osaka 560-0043, Japan*

(Received 27 October 2006; revised manuscript received 18 January 2007; published 9 July 2007)

Nuclear magnetic resonance (NMR) and nuclear quadrupole resonance (NQR) experiments have been performed on a single crystal of tetragonal $NpCoGa_5$, an itinerant antiferromagnet with a Néel temperature T_N =47 K. The antiferromagnetic phase is inverted to a field-induced ferromagnetic (FIF) phase with an applied field (H_0) above H_m ($T\rightarrow 0$) ~40 kOe oriented along the c axis. NMR spectra have been measured above and below T_N with $H_0 \| c$ and a axes and have been assigned to $^{69,71}Ga$ nuclei on two crystallographically inequivalent $1c$ and $4i$ sites and to ^{59}Co nuclei on the $1b$ site. Using second-order perturbation calculations, Knight shift (K), electric field gradient (EFG), frequency (ν_Q), and asymmetry parameter (η) of the EFG are deduced for each site. These parameters for the $^{69}Ga(1c)$ and $^{69,71}Ga(4i)$ sites are confirmed by NQR measurements in zero field. The Knight shifts obtained in the paramagnetic (PM) state obey a Curie-Weiss law, which scales with the bulk susceptibility (χ). Hyperfine tensors for each site are deduced from K-χ plots with temperature as an implicit parameter. Antiferromagnetic NMR spectra in zero field were also observed, finding an internal field of ~20 kOe at the Ga($4i$) site at the lowest temperature. The ordered moment can be estimated from this to be 0.81 μ_B/Np. The nuclear quadrupolar parameters (ν_Q and η) are found to exhibit an anomaly just below T_N in the FIF phase. T_1 and T_2 have been measured for each site. For $H_0 \| c$, $T_1 \sim$ constant behavior suggests localized $5f$ character for $T>100$ K and itinerant ($1/T_1 \propto T$) behavior for $T_N < T < \sim 100$ K in $NpCoGa_5$. T_2 measurements in the case of $H_0 \| c$ clearly define a phase crossover between PM and FIF phases. A sharp anisotropy for spin fluctuations in $NpCoGa_5$ has also been demonstrated.

DOI: 10.1103/PhysRevB.76.024410 PACS number(s): 75.30.Kz, 75.40.Gb, 75.50.Ee, 76.60.−k

I. INTRODUCTION

The recent discovery of the plutonium superconductors $PuCoGa_5$ (Ref. 1) and $PuRhGa_5$ (Ref. 2) with transition temperatures T_c=18 and 9 K, respectively, has excited a good deal of interest in the actinide-based (An115) compounds $AnTGa_5$ (An=U, Np, Pu; T=transition metal elements). An115 compounds crystallize in the tetragonal $HoCoGa_5$-type structure (space group $P4/mmm$), illustrated in Fig. 1(a). This crystal structure is quasi-two-dimensional in character, i.e., can be regarded as a sequential stacking of $AnGa_3$ and TGa_2 layers along the c axis. For some time now, the isostructural cerium-based series $CeTIn_5$ (T=Co, Rh, Ir), the so-called Ce115 systems, have been in the limelight, since they are heavy-fermion superconductors. T_c values for $CeCoIn_5$ and $CeIrIn_5$ are 2.3 and 0.4 K, respectively.[3–5] As for $CeRhIn_5$, which is an antiferromagnet with Néel temperature T_N=3.8 K at ambient pressure, it has been reported at first that the superconductivity appears around 2 K, along with suppression of the antiferromagnetic (AF) order, under applied pressure of $P^* \sim 2$ GPa.[6] Very recently, by means of ac-susceptibility measurements, this pressure-induced superconductivity in $CeRhIn_5$ has been suggested to coexist with the AF order (even at ambient pressure) in the pressure range of $P \lesssim P^*$.[7] Systematic nuclear magnetic resonance (NMR) investigations of the Ce115 systems have established that these superconductors have d-wave superconducting gaps[8–11] and that AF spin fluctuations play an active role in the superconducting pairing.[12–15] In the Pu115 systems, NMR measurements have yielded d-wave-like superconducting gap behavior,[16,17] while T_c values are an order of magnitude higher than those for the Ce115. On the other hand, in the U115 and Np115 series, which are Pauli paramagnets or antiferromagnets, no superconductivity has been found so far.[18–25] As a rule, the Np115 systems show a tendency to have complicated AF magnetic order, e.g., canted magnetic moments, double AF transitions, and/or additional magnetic moments on the transition metal elements.[25–30] Theoretical considerations suggest that peculiar magnetic behavior such as that found in the Np115 systems may be related to $5f$ quadrupolar interactions or orbital correlations.[31,32]

In order to understand the origin of exotic magnetism and superconductivity in the An115s, it is important to study member compounds having different numbers of $5f$ elec-

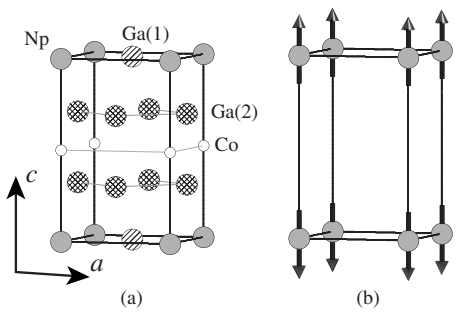

FIG. 1. (a) Crystal structure of $NpCoGa_5$. (b) Magnetic structure determined by neutron diffraction measurements (Ref. 34).

trons in a systematic way, such as $UCoGa_5$, $NpCoGa_5$, and $PuCoGa_5$. Here, $UCoGa_5$ is a Pauli paramagnet with a Sommerfeld coefficient of $\gamma \sim 3$ mJ/mol K^2.[21] The de Haas–van Alphen (dHvA) experiments have revealed that the Fermi surface of $UCoGa_5$ consists of small, closed regions corresponding to a semimetal.[21] These experimental dHvA frequencies are well explained by the $5f$-itinerant band model. On the other hand, $NpCoGa_5$, for which $\gamma \sim 60$ mJ/mol K^2 is moderately enhanced, shows AF order below $T_N=47$ K.[24,33] Neutron diffraction measurements have revealed that the AF wave vector $\boldsymbol{Q}$ is $(0,0,1/2)$ and that the ordered moment is 0.8 μ_B/Np parallel to the c axis.[34] This magnetic structure is illustrated in Fig. 1(b). Similar AF magnetic structure is found in the related system $UPtGa_5$.[19] The AF phase of $NpCoGa_5$ has been found to be metamagnetic along the c axis, i.e., becomes a field-induced ferromagnet (FIF) at fields higher than $H_m \sim 40$ kOe.[33,34] Through dHvA measurements, it has been shown that the FIF-phase Fermi surface consists of two main cylindrical sheets and some small pocket regions.[35] The large cyclotron masses revealed by this dHvA experiment suggest that $5f$ electrons contribute significantly to the conduction bands. On the other hand, dHvA oscillations observed in the AF state of $NpCoGa_5$ can be understood on the basis of an itinerant $5f$ electron model. As for the superconductor $PuCoGa_5$, which also has a moderately enhanced $\gamma \sim 100$ mJ/mol K^2,[1] band calculations have established that it has similar cylindrical Fermi surfaces.[36,37]

Recently, we have completed a series of NMR/nuclear quadrupole resonance (NQR) measurements on the ^{69,71}Ga and ^{59}Co nuclei in $NpCoGa_5$. NMR/NQR measurements are useful tools for characterizing the electronic states of such systems. Moreover, since $NpCoGa_5$ has only a single T_N, $NpCoGa_5$ may be classified as a rather simple object among other Np115 compounds having multiple phase transitions. Thus, this system establishes a good foundation for understanding other Np115 and An115 systems. In this paper, we report the NMR hyperfine (HF) parameters and relaxation rates of $NpCoGa_5$ in detail.

In Sec. II, the experimental details are given and the HF parameters are defined. Next, in Sec. III A, we report the static magnetic response in $NpCoGa_5$. This section comprises the following (1)–(6) sections: (1) The anisotropic H-T phase diagrams in $NpCoGa_5$ are summarized via magnetization measurements. (2) The NMR spectra obtained under high fields in the paramagnetic state are shown. (3) The temperature variations of those spectra through T_N are shown. Here, in Secs. III A 1 and III A 2, NMR line assignments and HF parameter determinations are given. (4) The temperature dependence of Knight shifts in the paramagnetic state are exhibited. Knight shifts are important, because from them, the transferred HF coupling tensors are deduced. (5) The results of zero field experiments are reported. In particular, quadrupole frequencies are derived from the NMR studies, and Ga NQR lines are then observed in the paramagnetic state. Then, below T_N, AFNMR lines are observed and analyzed. (6) The temperature dependence of nuclear quadrupolar parameters is obtained in the paramagnetic and ordered states. Here, a large coupling between magnetic polarization and the lattice in $NpCoGa_5$ is put into evidence.

Next, in Sec. III B, nuclear relaxation times in $NpCoGa_5$ are discussed in the following sections: (1) longitudinal nuclear relaxation rates $1/T_1$ and (2) transverse nuclear relaxation rates $1/T_2$. Here, the apparent nature of $5f$ electrons in $NpCoGa_5$ is found to vary from localized for temperatures above ~ 100 K and itinerant for temperatures below ~ 100 K; i.e., the AF state in $NpCoGa_5$ appears to be driven by itinerant $5f$ electrons. Spin fluctuations in the paramagnetic state are also shown to be highly anisotropic. Finally, in Sec. IV, a brief summary of the NMR/NQR results is given along with the H-T phase diagram of $NpCoGa_5$.

II. EXPERIMENT

Single-crystal samples of $NpCoGa_5$ were prepared by the Ga-flux method.[33] A single crystal with dimensions of $3 \times 3 \times 5$ mm^3 was used for the NMR/NQR measurements. This sample was selected from the same batch as was used for magnetic susceptibility,[33] dHvA,[35] and neutron diffraction[34] measurements.

Magnetization and magnetic susceptibility were measured using a superconducting quantum interference device magnetometer with applied fields of up to 55 kOe along the a or c axis of the single crystal. Magnetic susceptibility (χ) below T_N was defined here as the magnetization (M) divided by the applied field (H_0), i.e., $\chi \equiv M/H_0$.

NMR measurements were carried out in the temperature range 1.5–300 K using a phase-coherent, pulsed spectrometer installed in a special area for handling radioisotopes. The sample was mounted in a NMR coil; this assembly was set in epoxy cement and wrapped with polyimide tape. Field-swept NMR spectra were measured at a constant frequency with the applied field H_0 along either the a or c axis. Using these results, nuclear HF parameters were determined to sufficient accuracy using second-order perturbation theory. Quadrupolar parameters deduced from NMR were checked with frequency-swept NQR spectra using the same single-crystal sample. Frequency-swept spectra were measured in the limited frequency range of 15–30 MHz (zero field). With this scheme, several NQR lines in the paramagnetic (PM) phase and AFNMR lines in the AF phase were recorded.

Using conventional notation, the quadrupole frequency parameter is defined as $\nu_Q \equiv \frac{3e^2qQ}{2I(2I-1)h}$, where eQ is the nuclear quadrupolar moment, I is the nuclear spin quantum number, and $eq \equiv V_{ZZ}$ is the principal component of the electric field gradient (EFG) tensor. Here, V_{ii} denotes EFG tensor components in the principal coordinate system, such that $|V_{XX}| \leq |V_{YY}| \leq |V_{ZZ}|$ for each ionic site. The EFG components satisfy Laplace's equation, i.e., $V_{XX}+V_{YY}+V_{ZZ}=0$. The EFG asymmetry parameter is defined as $\eta \equiv \frac{|V_{YY}|-|V_{XX}|}{|V_{ZZ}|}$. If $\eta=0$, the NQR frequency ν_{NQR} for $I=3/2$ is simply equal to ν_Q; otherwise, $\nu_{NQR}=\nu_Q(1+\eta^2/3)^{1/2}$. Nuclear gyromagnetic ratio values used here are $^{59}\gamma_N/2\pi=1.0054$ MHz/kOe, $^{69}\gamma_N/2\pi=1.0220$ MHz/kOe, and $^{71}\gamma_N/2\pi=1.298\,55$ MHz/kOe.

The nuclear spin-lattice relaxation time T_1 was measured using the inversion-recovery method with a π pulse. Values of T_1 were obtained from fits to an appropriate relaxation function. The magnetization recovery $[\{M(\infty)-M(t)\}/M(\infty)]$ for the center and satellite NMR lines of the ^{69,71}Ga ($I=3/2$) nuclei gave satisfactory fits to the

single-T_1 functions $0.1\exp(-t/T_1)+0.9\exp(-6t/T_1)$ and $0.1\exp(-t/T_1)+0.5\exp(-3t/T_1)+0.4\exp(-6t/T_1)$, respectively. T_1 recovery for the ^{69,71}Ga NQR lines was a good fit to a single exponential, i.e., $\exp(-3t/T_1)$. In the same manner, the recovery function for the center line of ^{59}Co was adopted as $0.714\exp(-28t/T_1)+0.206\exp(-15t/T_1)+0.068\exp(-6t/T_1)+0.012\exp(-t/T_1)$. The value of the nuclear spin-spin relaxation time (T_2) was obtained by monitoring the spin-echo amplitude $M(2\tau)$ as a function of time 2τ between the first pulse and the echo. The $M(2\tau)$ data obtained were fitted to an exponential decay curve $M(0)\exp(-2\tau/T_2)$.

III. RESULTS AND DISCUSSION

A. Static magnetic response in $NpCoGa_5$

1. Static magnetic susceptibility and the phase diagram

$NpCoGa_5$ shows a characteristic anisotropy in electrical resistivity (ρ) and magnetic susceptibility (χ), which may relate to the quasi-two-dimensionality in this system.

As for ρ, ρ_c is approximately four times larger than ρ_a. ρ_a and ρ_c for $NpCoGa_5$ are nearly independent of temperature in the PM region above ~100 K.[33] The ρ-T curve is flat above ~100 K but gradually declines below ~100 K. With further temperature decrease, it shows a sharp drop below T_N.

The anisotropy of χ is also quite large in this compound; i.e., the c component of susceptibility is much larger than the a component in the PM state. In Fig. 2, $\chi_a(T)$ and $\chi_c(T)$ taken with H_0=10 kOe are shown as a function of temperature T. The PM susceptibilities obey Curie-Weiss laws above T_N, where the effective moments and the Weiss temperatures are estimated to be 2.70 μ_B/Np and −91 K for the c direction and 2.56 μ_B/Np and −239 K for the a direction, respectively. These effective moments are close to the ground-state value of 2.68 μ_B/Np for Np^{3+} ($5f^4$), but far from 3.62 μ_B/Np for Np^{4+} ($5f^3$).[33] Indeed, the temperature dependence of χ can be reproduced by a calculation on the basis of a Np^{3+} crystalline electric field (CEF) scheme, which can explain the anisotropy of χ in the PM region. However, the saturated moment of 0.74 μ_B/Np as shown in Figs. 2(b) and 2(c) and the ordered moment of 0.8 μ_B/Np as obtained by the neutron diffraction technique are sharply reduced from the effective moment mentioned above, or from the saturated moment in the CEF picture. This reduced moment indicates the delocalization of $5f$ electrons.

With $H_0\|c$, a very sharp metamagnetic transition from AF to FIF is clearly seen as shown in Fig. 2(c). On the other hand, with $H_0\|a$, the metamagnetic transition disappears entirely. These M-H_0 curves along the c axis sharply contrast with that for the related compound $UPtGa_5$, which has the same magnetic structure with very small ordered moment of 0.24 μ_B/U, in spite of the large effective moment of 1.1–1.8 μ_B.[18] In $UPtGa_5$, a metamagnetic transition has also been observed in the case of $H_0\|c$. However, the metamagnetic field is as large as H_m~530 kOe at 4.2 K.[38] In $UPtGa_5$, however, a remarkable increase of M is seen above H_m,

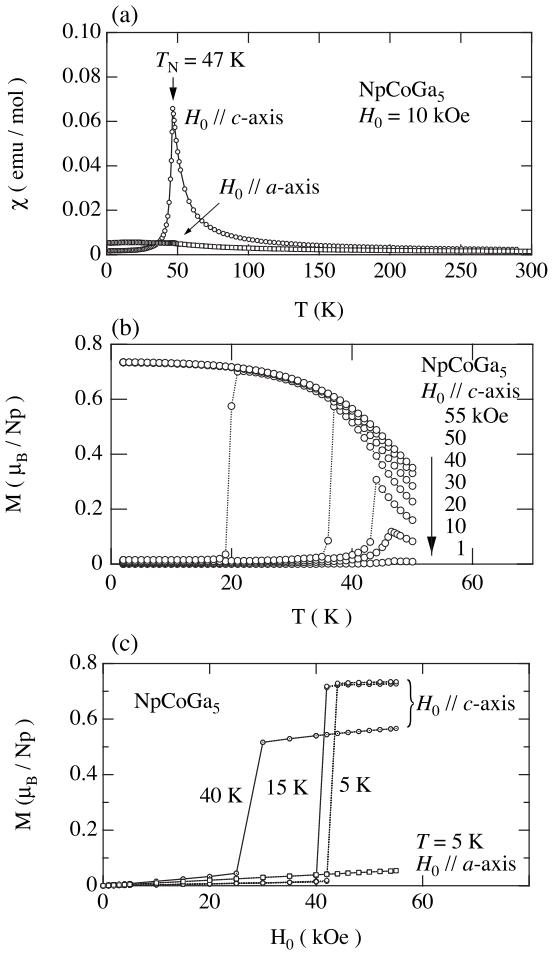

FIG. 2. (a) Temperature dependence of magnetic susceptibility of $NpCoGa_5$ with an external field (H_0) of 10 kOe parallel to the a and c axes. (b) H_0 variation of M-T plot with the field direction of $H_0\|c$. (c) M-H_0 curves along the a-axis (T=5 K) and the c axis (T=5, 15, and 40 K). See Ref. 33.

which can be understood on the basis of the spin-polarized $5f$-itinerant band magnetism. On the other hand, for $NpCoGa_5$, at fields above H_m, M is very nearly constant. This suggests that the $5f$ magnetism in $NpCoGa_5$ has more of a localized character than that in $UPtGa_5$.

The H-T phase diagram determined by magnetization measurements is shown in Fig. 3. The T_N in the case of $H_0\|a$ is determined by the sharp drop in the M-T plot. Except for the boundary between the PM and FIF states, the phase boundaries have also been confirmed by neutron diffraction measurements.[34] A ferromagneticlike M-T curve is also observed in the case of $H_0\|c$ for $H_0>H_m$, as shown in Fig. 2, the inflection points from which are plotted as a dotted line in Fig. 3. These points are seen to lie at $T\sim T_N$. It should be noted that specific heat measurements in applied fields show no clear anomaly[34] at the dotted line temperature in Fig. 3, which suggests that no second-order transition occurs here, but only a crossover from PM to FIF. This region will be re-examined with NMR measurements in the next sections.

2. NMR spectra in the PM state at fields above H_m

We have observed numerous NMR lines in the PM region and made assignments to ^{69,71}Ga and ^{59}Co nuclei on the re-

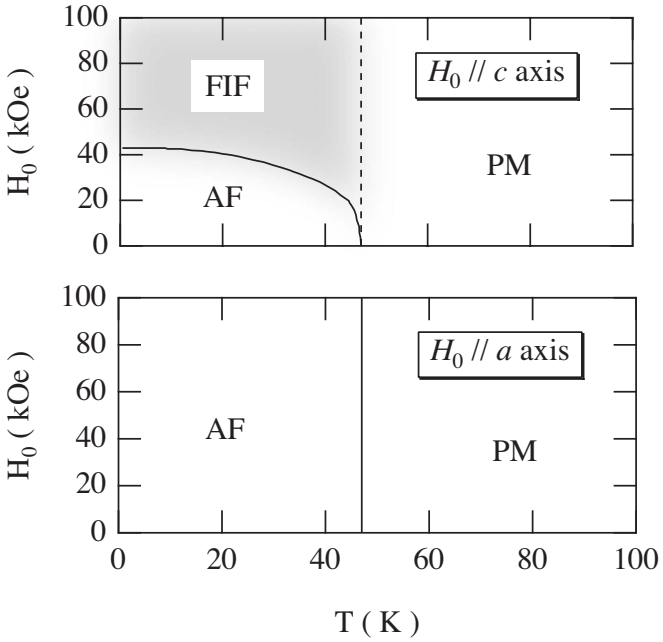

FIG. 3. Schematic *H-T* phase diagram for $NpCoGa_5$. The top and bottom panels show the cases of $H_0 \| c$ and $\| a$, respectively (see Refs. 33 and 34).

spective sites as follows. Figure 4 shows field-swept NMR spectra at 100 K in the PM state, measured for $H_0 \| c$ and a, respectively. Assignments to sites and nuclear species are also shown in this figure.

To explain these assignments, we first describe the site symmetries and the relationship to the applied field (H_0) of the observed nuclei, ^{69}Ga ($I=3/2$), ^{71}Ga ($I=3/2$), and ^{59}Co ($I=7/2$). First of all, as seen in Fig. 1(a), the Co(1*b*) sites, which lie between Ga layers, have fourfold axial symmetry along the *c* axis. Thus, with $H_0 \| c$, seven equally spaced NMR lines should be observed for the ^{59}Co. For $H_0 \perp c$ at frequencies large compared with the quadrupole splitting, one will find seven lines again with approximately half of the *c* axis splitting. These features are clearly observed in Fig. 4.

There are two crystallographically inequivalent Ga sites denoted by Ga(1) (1*c* site) and Ga(2) (4*i* site). The Ga(1) sites have axial symmetry in the Np-Ga planes, while the Ga(2) sites have two Np and two Co neighbors in the *a* planes and, thus, lower symmetry. For the Ga(2), the principal EFG axis (V_{ZZ}) is perpendicular to the *a* plane. With $H_0 \| c$, the Ga(2) sites are equivalent. With $H_0 \| a$, the Ga(2) sites divide into two magnetically inequivalent sites, i.e., Ga(2a) and Ga(2b) (see Fig. 4), where (2a) and (2b) means H_0 is parallel and perpendicular to the EFG principal (a) axis, respectively. For each Ga site, there are three NMR lines (one center and two satellite lines). For the Ga(1) sites with $H_0 \| c$, the three lines have equal spacing, so these are easy to identify. With $H_0 \perp c$ (a axis), the Ga(1) lines have a roughly equal spacing which is about half that for $H_0 \| c$. The Ga(2) lines are easy to spot, because they are much more intense than the Ga(1). However, for the Ga(2), the spacings are not equal, the center line being displaced toward the lower field in a field-sweep spectrum. For $H_0 \| a$, there are

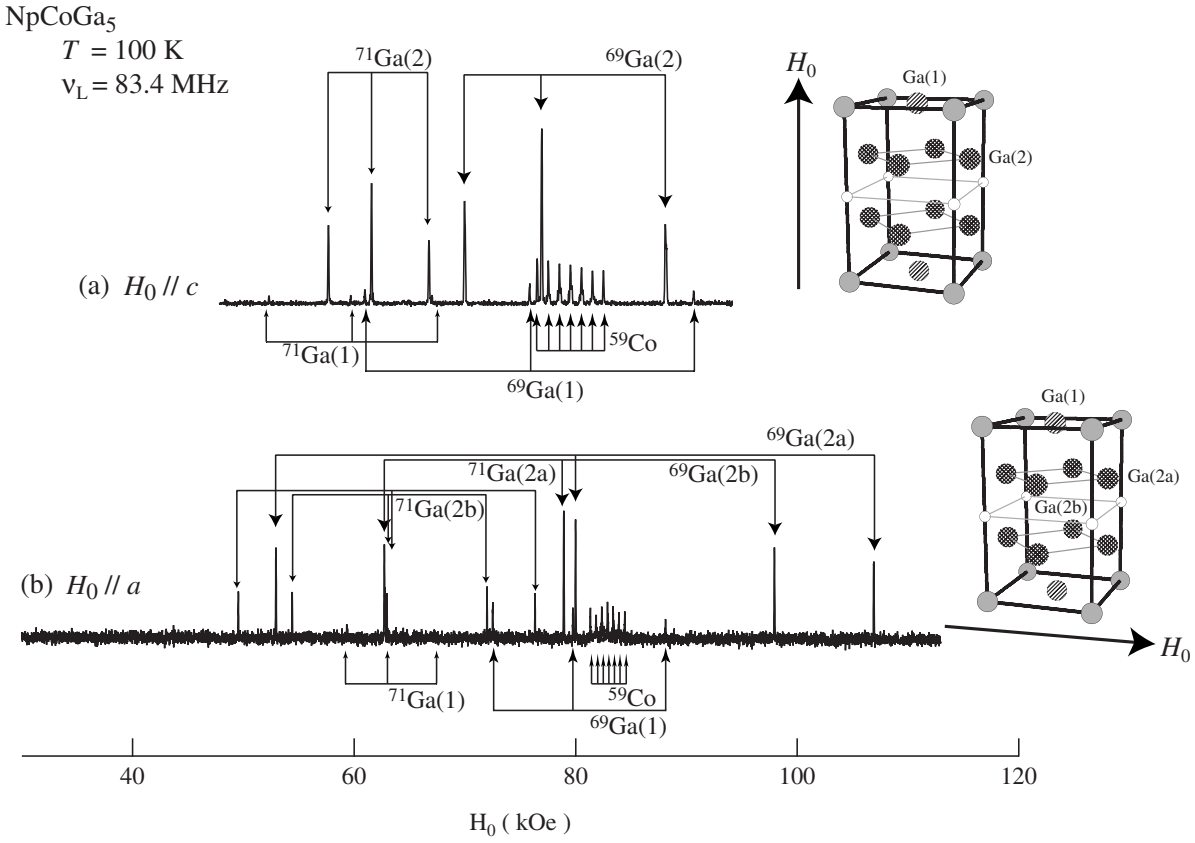

FIG. 4. Field-swept NMR spectra of $NpCoGa_5$ at 100 K with external field (H_0) along (a) the *c* axis and (b) the *a* axis, respectively. Sketches of the unit cell show the field directions relative to crystal axes. Assignments of the NMR lines are indicated by arrows.

two magnetically inequivalent Ga(2) sites (see Fig. 4), so that there are 12 Ga(2) lines in Fig. 4(b). Using the above considerations and the fact that the satellite spacings for the two isotopes stand in proportion to their respective quadrupole moments, the assignments in Fig. 4 have been determined.

Following these assignments, second-order perturbation calculations based on ^{69,71}Ga(1) resonant fields for $H_0 \| c$ provide values of the Knight shifts $^{69,71}K(1)$, quadrupolar frequencies $^{69,71}\nu_Q$, and the zenith angle θ relative to the principal axis (c axis). The ^{59}Co set also yields ^{59}K, $^{59}\nu_Q$, and θ. These calculations have been performed using the simultaneous equations given in Ref. 39. For $H_0 \| c$, θ should be $\simeq 0°$, and for $H_0 \| a$, it should be $\simeq 90°$. In both cases, the values of θ found included misalignment errors of 1°–3°. After finding the θ value from the Ga(1) results, perturbation calculations have been done for the ^{69,71}Ga(2) sets, yielding values of $^{69,71}K(2)$, $^{69,71}\nu_Q(2)$, $\eta(2)$, and the azimuth ϕ. A cross-check of calculated values has also been performed by comparing isotopes, where the experimental quadrupolar parameters should satisfy the relation $^{69}\nu_Q/^{71}\nu_Q \approx {}^{69}Q/{}^{71}Q = 1.5846$.

Here, it may seem that exact diagonalization, as used below in Sec. III A 5, would be better than second-order perturbation calculations for the determination of the HF parameters. However, values obtained by the diagonalization method are very nearly the same as second-order perturbation calculations in these high field cases, and the HF parameters derived from perturbation calculations have been confirmed by measured NQR frequencies, as described below in Sec. III A 5. Moreover, numerical diagonalization is far more cumbersome for obtaining the fitted values of many parameters, as seen in Sec. III A 5. We also note that this method has been very successful for the U115 systems.[40–43] The present results for shift and quadrupolar parameters will be discussed in detail in Secs. III A 4 and III A 6

3. NMR spectra below T_N in fields greater than H_m

As described above in Sec. III A 1, for $H_0 \| c$, a metamagnetic transition between AF and FIF states is seen below T_N. The metamagnetic field H_m increases as temperature decreases below T_N, reaching a maximum of approximately 40 kOe, as shown in Fig. 3. We have also found that a crossover line between PM and FIF states exists at $\sim T_N$. The spectral change through this crossover line is seen in Fig. 5, which shows NMR spectra using applied fields above 40 kOe at several temperatures above and below T_N with $H_0 \| c$.

As seen in Fig. 5, NMR lines do not show any sudden change, i.e., line splittings or sudden jumps, as the temperature goes below T_N. All the NMR lines shift to sharply lower resonance fields with lowering temperature, indicating that the Knight shift at each site increases smoothly, but substantially, through T_N. In other words, each site feels an additional HF field parallel to H_0. Since the NMR spectra in the FIF phase are similar to those in the PM phase, K values and the nuclear quadrupolar parameters can be evaluated straightforwardly. It is noted that all the linewidths are enlarged around T_N, corresponding to increases in the relaxation rates $(1/T_2)$ as described in Sec. III B 2.

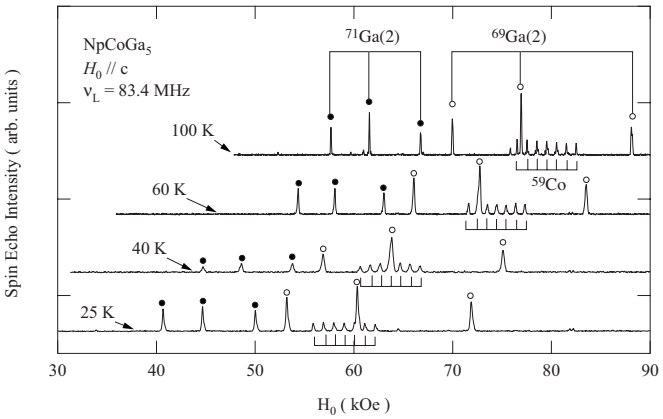

FIG. 5. Temperature variation of NMR spectra for $H_0 \| c$. For clarity, the ^{69}Ga(2) and ^{71}Ga(2) assignments are displayed by open circles (○) and closed circles (●), respectively. The ^{59}Co assignment is also shown.

Figure 6 shows the temperature variation of NMR spectra in the case of $H_0 \| a$. In this case, $NpCoGa_5$ enters the AF phase below T_N. For clarity an expanded view of the central region is shown in Fig. 7. Note that the seven lines of ^{59}Co do not shift below T_N. Thus, any internal field in the ordered state seems to cancel out at the Co sites. On the other hand, each Ga line undergoes a small splitting below T_N. At 25 K, the splittings of ^{69}Ga(2a) and ^{69}Ga(2b) are ~ 1.0 and ~ 1.5 kOe, respectively. As determined below from AFNMR results, the transferred field at the Ga(2) site reaches ~ 20 kOe as $T \to 0$. Owing to this large transferred field, a few degrees of field misorientation produce the observed NMR splitting (Fig. 7) at the Ga(2) site. The corresponding misalignment angle was estimated to be 1°–3° in this experiment, which is equal to that estimated from the PM state data.

4. Temperature variation of Knight shifts

In Fig. 8, Knight shifts K_c and K_a for the cases of $H_0 \| c$ and a, respectively, are shown for the ^{69}Ga(1), ^{69}Ga(2), and

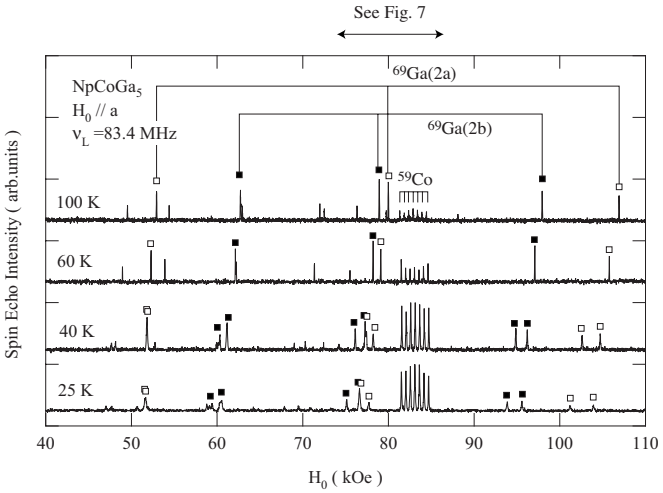

FIG. 6. Temperature variation of NMR spectra in the case of $H_0 \| a$. For clarity, the assignments of ^{69}Ga(2a) and ^{69}Ga(2b) are shown by open squares (□) and closed squares (■), respectively.

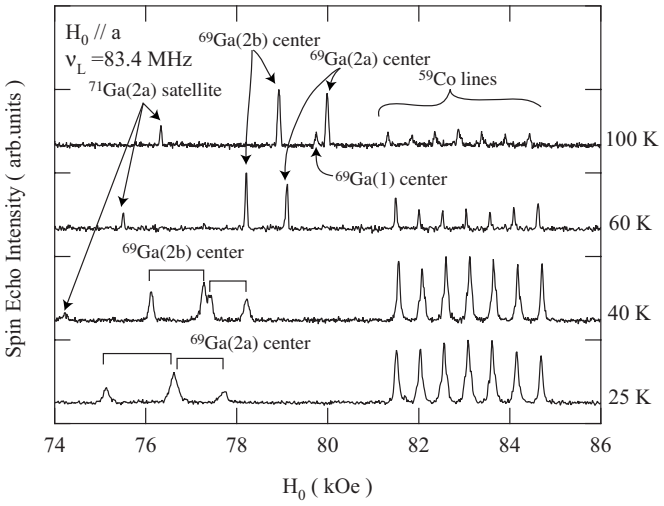

FIG. 7. Enlargement of Fig. 6 near the center lines of ^{69}Ga(2a), ^{71}Ga(2b), and ^{59}Co.

^{59}Co sites. We note that the parameters below T_N, shown as a gray region in Fig. 8, have been calculated using the NMR data for the case of $H_0 \| c$. All Knight shifts on the Co and Ga sites increase as temperature decreases in the PM state, except for the $^{59}K_a$ which decreases. In the FIF state, as temperature decreases below T_N, the Knight shifts increase and saturate at low temperatures. This behavior corresponds to the temperature dependence of bulk M $(H > H_m)$.

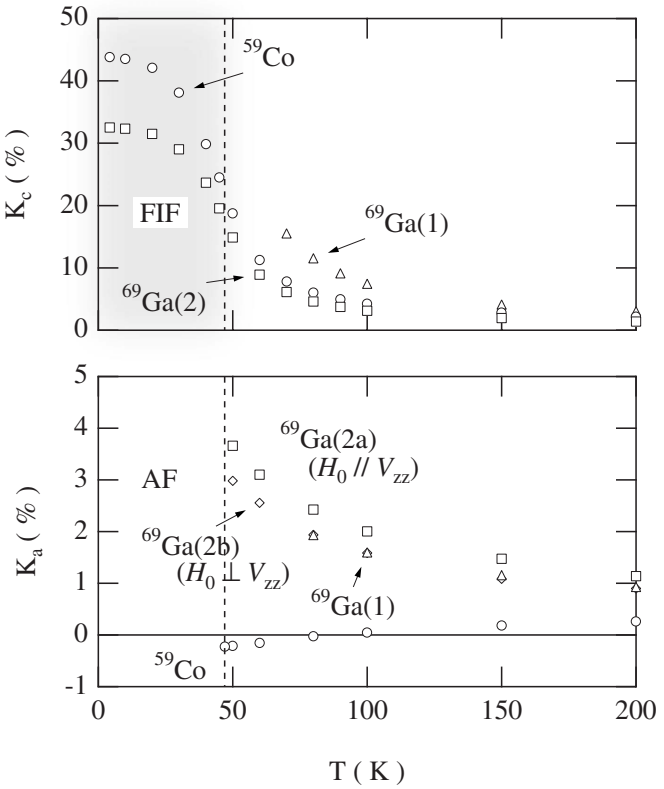

FIG. 8. The temperature dependence of Knight shift for ^{69}Ga(1), ^{69}Ga(2), and ^{59}Co. Top and bottom panels are for $H_0 \| c$ and a, respectively.

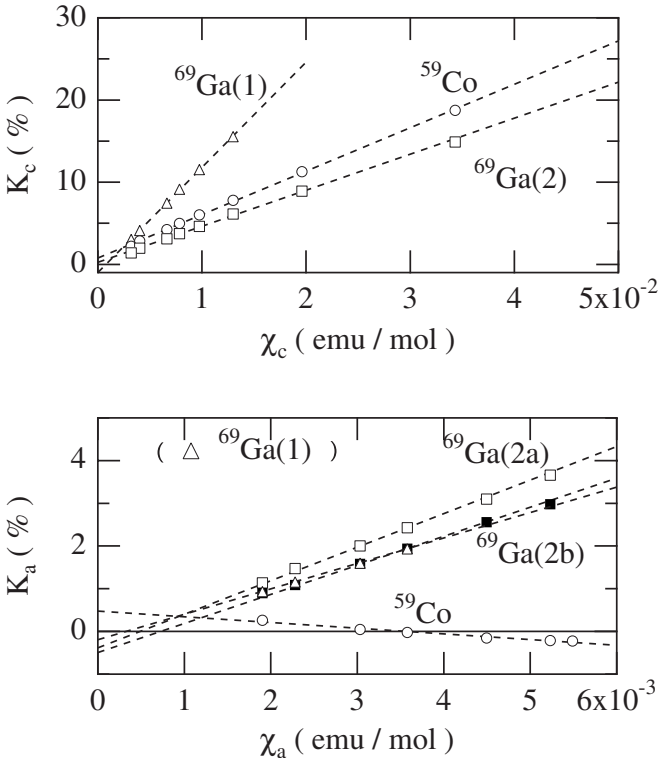

FIG. 9. K-χ plot for the various sites in $NpCoGa_5$. The upper and lower panels show plots for $H_0 \| c$ and a, respectively.

Figure 9 presents the so-called K-χ plots for shift data from Fig. 8 (PM region), with temperature as an implicit parameter. In recent empirical analyses,[45] K-χ bending anomalies are found to occur widely in heavy-fermion systems. This presumably has to do with the condensation of heavy-fermion liquids at low temperatures. Otherwise, such K-χ bending has often been explained by thermal depopulation of CEF levels.[10,44] The linear K-χ behavior which we find for $NpCoGa_5$ may suggest rather localized character for the $5f$ electrons and/or a larger separation between ground and excited CEF levels.

From the slopes of the K-χ plots, transferred HF coupling constants have been straightforwardly obtained and are summarized in Table I. These highly anisotropic HF couplings are related to hybridization between Np $5f$ and Ga $4p$ bands and between Np $5f$ and Co $3d$ bands near the Fermi surface.

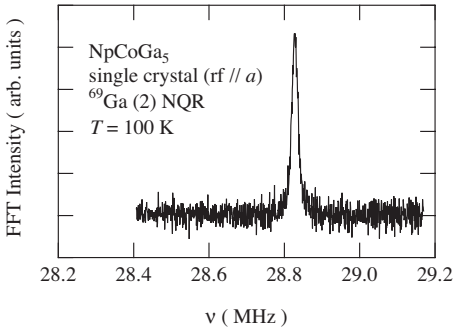

FIG. 10. NQR spectral line assigned to ^{6}Ga(2) in zero field at 100 K.

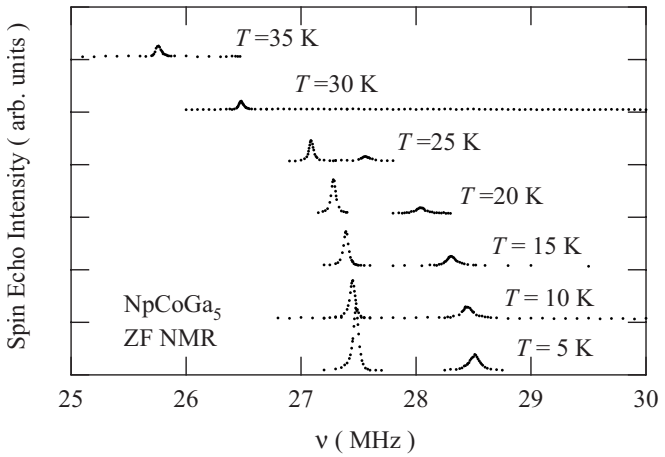

FIG. 11. Temperature variation of AFNMR spectra in zero field.

Interestingly, the transferred hyperfine couplings on the Ga(1), Ga(2), and Co sites seem to increase with distance from the Np site. This also suggests that the strength of hybridization with $5f$ bands would be reflected in the amplitude of the HF coupling on the respective site.

5. Zero field experiments

Generally, zero field (ZF) NQR experiments require powder specimens in order to increase the surface penetration of rf fields. In the present case, the preparation of such a powdered sample of a transuranium compound increases the experimental difficulties dramatically owing to strong radioactivity. Under the constraints attendant to radioisotopes, we use the same single crystal without crushing or grinding. The NQR signals for ^{69}Ga(1,2) and ^{71}Ga(2) in ZF have been detected using the same single crystal. Subsequently, we also

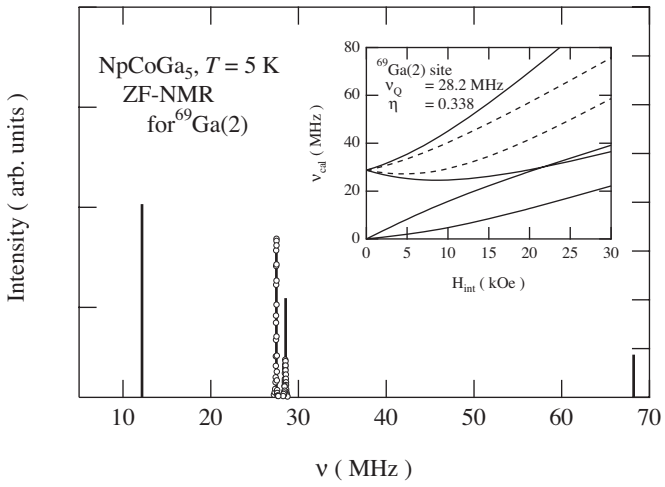

FIG. 12. Calculated AF NMR lines for ^{69}Ga(2) assuming $H_{\rm int}$ =19.4 kOe along the c axis, $\nu_{\rm Q}$=28.2 MHz, and η=0.338. The raw experimental data are also shown as open circles. The inset shows the $H_{\rm int}$ variation of calculated frequencies with fixed parameters $\nu_{\rm Q}$ and η. The solid and broken lines indicate resonant frequencies with finite and nearly zero intensities, respectively.

TABLE I. Transferred hyperfine coupling constants in the PM state from K-χ plots. Units are kOe/μ_B.

	$H_0 \| c$	$H_0 \| a$
^{69}Ga(1)	71.4±0.6	33.3±0.2
^{69}Ga(2)	24.5±0.5	(a) 43.9±0.3, (b) 38.0±1.3
^{59}Co	29.5±0.3	−7.5±0.6

succeeded in detecting the NMR signal of ^{69}Ga(2) in the AF phase at ZF.

Figure 10 shows the NQR line assigned to ^{69}Ga(2) at 100 K, where the rf field was applied along the a axis. The NQR spectra for ^{69}Ga(1) and ^{71}Ga(2) have also been measured (not shown). As seen in Fig. 10, the narrow ~20 kHz linewidth indicates a high quality sample, i.e., there are relatively few lattice defects and/or magnetic impurities. The observed NQR frequencies for ^{69}Ga(1,2) are very nearly equal to $\nu_{\rm Q}\sqrt{1+\eta^2/3}$ using data obtained from the NMR results. This result assures us that the analyses of NMR spectra are accurate.

Next, we turn to the AF ordered state in ZF. Two NMR lines can be found at 5 K, one at ≃27.5 MHz and one at ≃28.5 MHz, as shown in Fig. 11. The two NMR lines are barely observable in this experimental situation. The temperature variation of these lines is also shown in Fig. 11. These lines both shift gradually to lower frequencies as temperature increases from 5 to 30 K, and they eventually coalesce above 30 K. Above 35 K, such signals became too weak to detect, because the fast relaxation rates near T_N depress the signals in that region. If these signals were ascribed to ^{69}Ga(1) or ^{71}Ga(2), many lines should be observable. From our numerical calculation, the lines ascribed to ^{69}Ga(2) should have the largest intensities. The two lines can only be ascribed to ^{69}Ga(2), whereupon the internal field ($H_{\rm int}$) and quadrupolar parameters ($\nu_{\rm Q}$ and η) are estimated in the AF state as follows.

The AF structure has been determined by neutron scattering,[34] as shown in Fig. 1(b). This magnetic structure is the same as that of the related compound $UPtGa_5$.[19] As discussed in our previous report on $UPtGa_5$,[42] in this magnetic structure, the Ga(2) site has C_{2z} symmetry. Therefore, the direction of the internal field ($H_{\rm int}$) at the Ga(2) site should be fixed along the c axis, which coincides with V_{XX}. Moreover, the value of $|H_{\rm int}|$ extrapolated to $H_0 \to 0$ can be determined roughly from NMR experiments (not shown) in the AF state, i.e., with $H_0 < H_m$.

The determination of EFG parameters was done by numerical diagonalization of the effective Hamiltonian matrix including Zeeman and quadrupolar terms. Using the extrapolated $H_{\rm int}$ as an initial value, $\nu_{\rm Q}$ and η are calculated. An example of calculated results is shown in Fig. 12. The inset to Fig. 12 shows the variation of calculated frequencies with $H_{\rm int}$, assuming fixed quadrupolar parameters. All calculated resonance frequencies are plotted in this inset, where the solid and broken lines present the resonant frequencies with finite and nearly zero intensities, respectively. As shown in Fig. 12, four lines should be observed for ^{69}Ga(2) in the AF

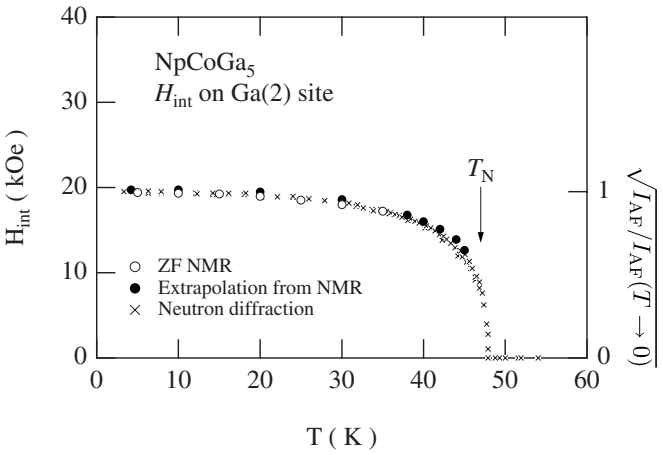

FIG. 13. Temperature variation of the internal field at the Ga(2) site. The normalized square-root intensities of AF Bragg peaks obtained using neutron diffraction techniques (Ref. 34) are also shown (right-hand scale).

state, although only two lines were observed in this experiment. Through a series of iterated diagonalizations, the best solution for $H_{\rm int}$, $\nu_{\rm Q}$, and η is found. We note that the $H_{\rm int}$ parameter hardly changes from the initial estimate throughout this procedure.

As seen in Fig. 13, the development of $H_{\rm int}$ below T_N is quite consistent with the neutron diffraction data.[34] The HF field at the Ga(2) site is estimated to be 19.8 kOe as $T \rightarrow 0$. Assuming that the HF coupling constant does not change from the PM state, the ordered moment on the Np site is estimated to be 0.81 μ_B, which agrees nicely with neutron data[34] as well as with a Mössbauer study.[24,34] From this result, the HF coupling constant in the AF state is concluded to be very nearly that of the PM state.

6. Temperature variation of nuclear quadrupolar parameters

The nuclear quadrupolar parameters obtained are summarized in Fig. 14. The deduced components of the EFG from these quadrupolar parameters for the Ga(2) and Co sites are plotted in Fig. 15. In both figures, values obtained both by NMR experiments in the FIF state and by ZFNMR in the AF state are plotted.

In the PM phase, the values obtained from NMR and NQR experiments are quite consistent. The temperature dependence of the quadrupolar parameters in the PM phase is very flat. On the other hand, just below T_N, the quadrupolar parameters of the Ga(2) sites show a sudden change with temperature, whereas those for the Co sites do not change so much through T_N. Moreover, the nuclear quadrupolar parameters in the AF state seem to deviate from the estimates obtained from the FIF state. In particular, the divergence of $\nu_{\rm Q}$ and η seems to be quite large near T_N. For example, as seen in Fig. 14, the $\nu_{\rm Q}$ at 35 K (near T_N) in the AF state is obtained as 26.4 MHz, although this $\nu_{\rm Q}(T)$ should connect around T_N to the paramagnetic value of ~28.2 MHz. On the other hand, $\nu_{\rm Q} \sim 28$ MHz in the FIF state just below T_N. Variation of the EFG between the FIF and AF states suggests a substantial coupling between the lattice and magnetic polarization.

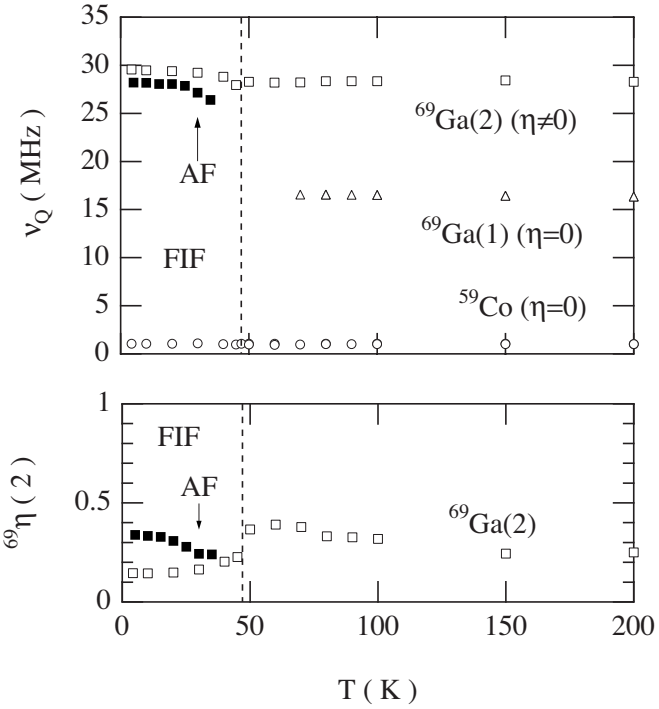

FIG. 14. Temperature dependence of nuclear quadrupolar parameters. In the upper panel, the quadrupole frequencies $\nu_{\rm Q}$ of ^{69}Ga(1), ^{69}Ga(2), and ^{59}Co are plotted. In the lower panel, the EFG asymmetry parameter η for ^{69}Ga(2) is shown. The open symbols (□, △, and ○) for the PM and FIF states and closed squares (■) for the AF state represent the data obtained by NMR and by ZFNMR, respectively.

The EFG may be decomposed into intra-atomic and interatomic contributions. The former piece, coming from unfilled valence states, mainly represents the symmetry of hybridized orbitals, whereas the latter part represents the lattice contribution. Tentatively, we estimate which contributions to EFG are important for each site as follows. Using a point charge model (assuming appropriate ionic charge state), the lattice contribution is estimated from $eq_{\rm lattice}(1-\gamma_\infty)$, where γ_∞ is the Sternheimer antishielding constant and $q_{\rm lattice} = \Sigma_j \frac{Q_j(3z_j^2 - r_j^2)}{r_j^5}$. In the literature,[46] $(1-\gamma_\infty)$ has been given as ~10 for the elements Co and Ga. Assuming room temperature values for the lattice parameters, we estimate $V_{ZZ} \sim 8 \times 10^{16} - 1 \times 10^{17}$ V cm^2 for the Co site (depending on charge states), which is close to the experimental value. This result indicates that the EFG at the Co site is mainly due to the interatomic part and that the intra-atomic part is negligible for this site. In other words, the Co atom does not exhibit any charge distribution on itself. It is entirely consistent with the band calculations which tell that the *d* band from Co atoms lies deep inside from the Fermi level.

In the same manner, the lattice contribution is estimated for the Ga(2) site to be $V_{ZZ} \sim (2-4) \times 10^{17}$ V cm^2, which is rather smaller than the experimental value. On the other hand, the intra-atomic part of V_{ZZ} at the Ga(2) site can be estimated from $q_{\rm intra} = (1-R) f(p_x, p_y, p_z) \langle r^{-3} \rangle$. Here, $1-R \sim 1.1$ is the antishielding factor for the Ga atom,[47] and

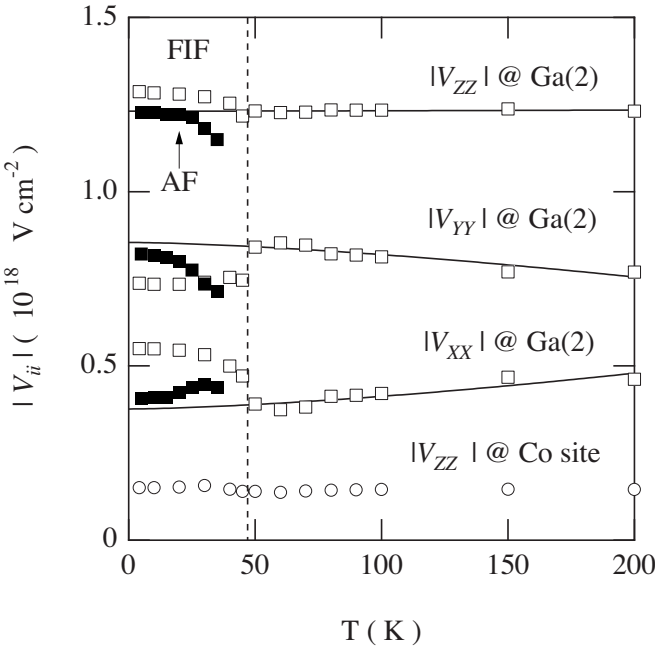

FIG. 15. Temperature dependence of EFG components for Ga(2) and Co sites. The open and closed symbols represent the deduced data from NMR and from ZFNMR, respectively. The dotted line is drawn at T_N=47 K. The solid curves are guides for the eyes.

$f(p_x,p_y,p_z)$ is a numerical factor ranging from 0 to 1, which is determined by the symmetry of the Ga(2) site and the occupation fractions for each of the $4p$ orbitals. Using $\langle r^{-3}\rangle_{4p}$=2.89 a.u. for the neutral atom,[48] $eq_{\text{intra}} \sim f(p_x,p_y,p_z)\times(3\times10^{18}$ V cm^2) is obtained, which is of the same order as the experimental value. These results suggest that both contributions are important for the EFG at the Ga(2) site.

Considering the change of EFG just below T_N, it is unlikely that such a change comes from the intra-atomic part, because the corresponding change of $f(p_x,p_y,p_z)$ means a change in the $4p$-$5f$ hybridization leading to a shift of HF coupling constants. No such shift is observed for $NpCoGa_5$, as described above. On the other hand, it may come from the lattice contribution. One expects there to be a magnetovolume effect in $NpCoGa_5$. Indeed, in the related U115 compounds, a certain amount of magnetostriction has been found,[49] although the changes of lattice parameters are limited to 0.05% at most. By estimates made with the point charge model, changes in the lattice parameters (a and c) of more than 5% would be required for such a change of EFG in $NpCoGa_5$. It may also be required that the structural parameter (z) of Ga(2) changes as well. Such lattice changes seem to be too large by comparison with U115 systems. Perhaps, in order to explain such a large change of EFG at the Ga(2) site, charge distributions on the Np sites related to $5f$ quadrupoles may have to be taken into account. Such a further analysis cannot be pursued at this point, since there are neither thermal expansion nor low-T x-ray diffraction experimental data.

In the end, we can only reiterate that the nuclear quadrupolar parameters show striking changes at T_N and that they are quite sensitive to magnetovolume effects and changes in hybridization between the Ga $4p$ and Np $5f$ electrons.

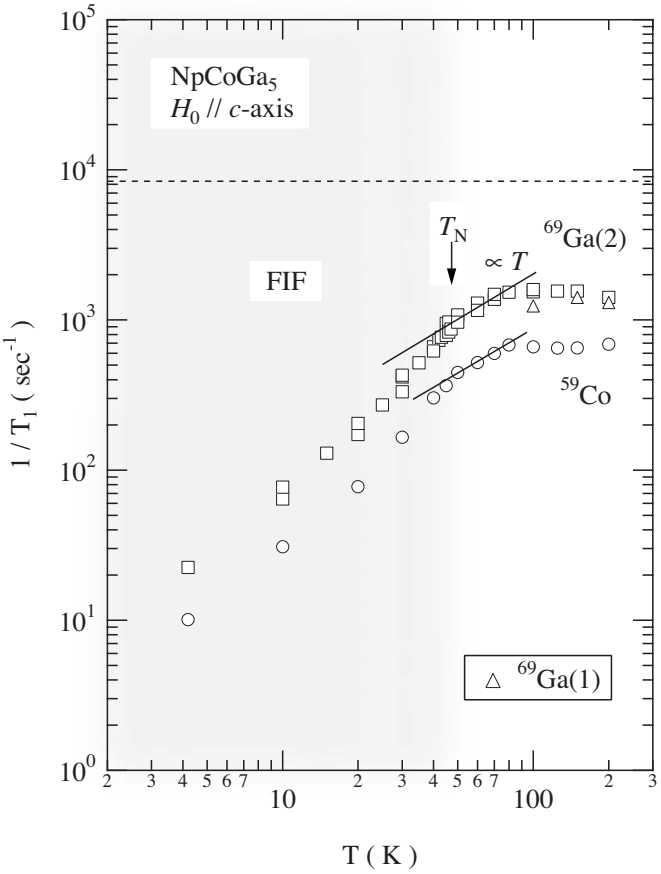

FIG. 16. Temperature dependence of nuclear spin relaxation rates for ^{59}Co, ^{69}Ga(1), and ^{69}Ga(2) for the case of $H_0\|c$. The dotted horizontal line represents a tentative estimate from the local moment model for ^{69}Ga(2) (see text). The solid lines represent $(T_1T)^{-1}$=constant behavior.

B. Dynamical magnetic response in $NpCoGa_5$

1. T_1 measurements

Nuclear spin-lattice relaxation times T_1 have been measured for the NMR lines of ^{59}Co, ^{69}Ga(1), and ^{69}Ga(2) for the cases of $H_0\|c$ and a, as shown in Figs. 16 and 17, respectively. T_1 data for ^{69}Ga(1,2) were taken on the higher satellite lines to avoid interference from the ^{59}Co-NMR lines. For the Ga(1) site, T_1 could not be measured below ~100 K, since the signal was greatly weakened by a diminishing T_2 value. In this section, we then focus on the T_1 results for the Ga(2) and Co sites.

It is clear that the T_1 processes in this system are driven by magnetic interactions, because we have checked the isotope ratio of $1/T_1$ for Ga(2): For the Ga(2) sites, T_1 has been measured for both isotopes in a number of cases, for each of which we find that $^{69}T_1/^{71}T_1 \approx (^{71}\gamma_N/^{69}\gamma_N)^2$.

As for the temperature dependence of $1/T_1$ for Ga(2) and Co, above ~100 K, the T_1 values are very nearly constant. Such a constant T_1 behavior in the high temperature range

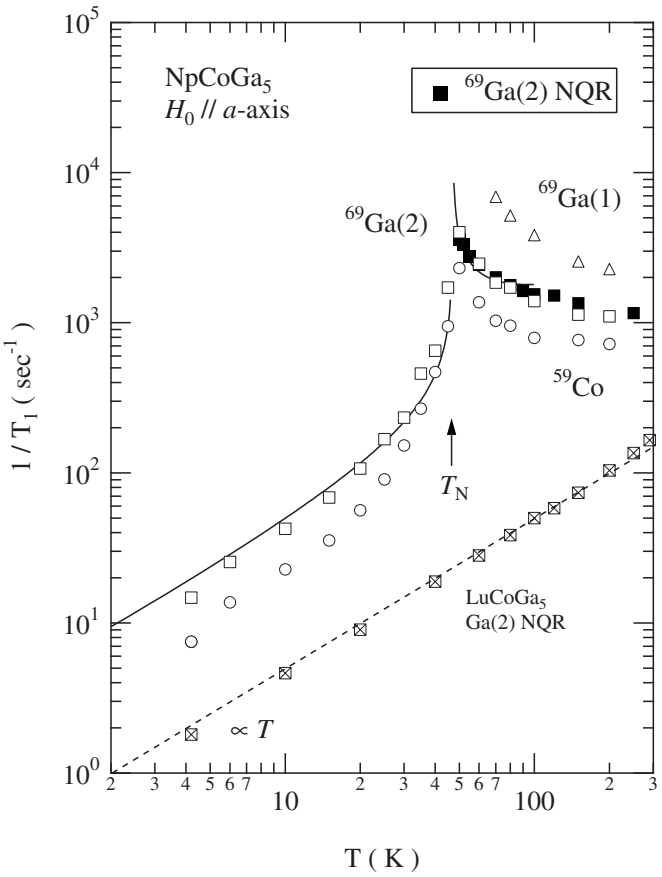

FIG. 17. Temperature dependence of nuclear spin relaxation rates for ^{59}Co, ^{69}Ga(1), and ^{69}Ga(2) for the case of $H_0 \| a$. T_1 data from ^{69}Ga(2) NQR (zero field) in $NpCoGa_5$ and $LuCoGa_5$ are also plotted. The dotted line for $LuCoGa_5$ NQR represents a $1/T_1T = 0.495$ (s K)$^{-1}$. The solid line represents a fit to the SCR theory of T_1 for an itinerant antiferromagnet (see text).

appears to reflect localized moment fluctuations for this system. Accordingly, we estimate T_1 in the exchange-narrowed limit. Assuming the simple case of exchange-coupled localized moments, the exchange frequency ω_{ex} may be estimated from the measured Curie-Weiss temperature (Θ from bulk-χ data) according to[50]

$$(\hbar\omega_{ex})^2 = (k_B\Theta)^2 \frac{3g_J}{z|g_J-1|^3 J(J+1)}, \tag{1}$$

where z is the number of nearest-neighbor magnetic ions (in this case, $z=4$ is adopted) and g_J is the Landé g factor. Using $J=4$ and $g_J=\frac{3}{5}$ for trivalent Np^{3+} ($5f^4$), ω_{ex} is estimated to be 1.9×10^{13} s^{-1}. The limiting T_1 is estimated assuming an isotropic HF coupling constant A_{iso},

$$\left(\frac{1}{T_1}\right)_{limit} = \sqrt{2\pi}\left(\frac{\gamma_N g_J \mu_B A_{iso}}{z'}\right)^2 \frac{z'J(J+1)}{3\omega_{ex}}, \tag{2}$$

where z' is the number of magnetic ions coupling to the ligand nucleus ($z'=2$), and $A_{iso}^2=(A_a^2+A_b^2+A_c^2)/3$ is used. Then, $(1/T_1)_{limit}$ for ^{69}Ga(2) is estimated to be 8.8×10^3 s^{-1}, as plotted in Fig. 16. In the same way, the limit for ^{59}Co is also estimated to be 2.1×10^3 s^{-1}. In fact, the experimental values are smaller than the exchange narrowing limit, indicating some degree of itineracy for the valence electrons, although the constant behavior of $1/T_1$ suggests a localized character.

In the case of $H_0 \| c$, as temperature decreases below 100 K, $1/T_1$ for ^{69}Ga(2) and ^{59}Co decrease at first linearly with T, and then decrease more steeply below T_N. This temperature threshold of ~100 K also coincides with the onset of a decrease in ρ,[25] as mentioned at the beginning of Sec. III A 1. From these results, the $5f$ electrons appear to behave in a more itinerant fashion below $T\sim100$ K. We also note here that, as with the shift results (Fig. 8), the PM-FIF transition is severely broadened by the applied field along the c axis. Thus, there is no peak in $1/T_1$, but merely a change in slope (see, however, the SCR theory of T_1 in ferromagnets[51]).

Generally, if the enhancement factor due to spin fluctuations is omitted, $(1/T_1T)$ is usually proportional to $\gamma_N^2\langle A\rangle^2 N(E_F)^2$, where $N(E_F)$ is the DOS at E_F and $\langle A\rangle$ means the $\boldsymbol{q}$ average of HF coupling constant at E_F. The values of $(T_1T)^{-1}_{H_0\|c}$ for ^{69}Ga(2) and ^{59}Co just above T_N are ~21.5 and ~8.9 (s K)$^{-1}$, which are reduced to ~5.3 and ~2.4 (s K)$^{-1}$, respectively, as $T\to0$. These results suggest that $N(E_F)$ decreases with the development of exchange polarization in the FIF state.

On the other hand, for $H_0 \| a$, as seen in Fig. 17, $1/T_1$ shows a critical slowing down peak at T_N because the applied field does not couple to the fluctuating AF order parameter. This divergence of $1/T_1$ can be fitted with the following functions from self-consistent renormalization theory for weak, itinerant antiferromagnets,[51]

$$\frac{1}{T_1} = \begin{cases} aT + \dfrac{bT}{\sqrt{T-T_N}} & (T>T_N), \\ aT + \dfrac{cT}{\sqrt{T_N-T}} & (T<T_N). \end{cases} \tag{3}$$

The first term in the above formula represents the Korringa term from noninteracting conduction electrons. In Fig. 17, the temperature variation of $1/T_1$ for Ga(2) NQR in $LuCoGa_5$ is also shown.[52] $LuCoGa_5$ can be thought as a good reference material for actinide 115 compounds, because Lu has a fully occupied $(4f)^{14}$ configuration. As a noninteracting value, the $a=0.495$ (s K)$^{-1}$ for $LuCoGa_5$ is adopted. From a fit to Eq. (3), the values $b=131$ and $c=30$ s^{-1} K$^{-1/2}$ are obtained.

As for $N(E_F)$ in this case, the $(T_1T)^{-1}_{H_0\|a}$ as $T\to0$ in the AF state is estimated to be ~3.5 (s K)$^{-1}$ for ^{69}Ga(2) or ~1.8 (s K)$^{-1}$ for ^{59}Co. Since $(T_1T)^{-1}_{H_0\|a}$ just above T_N is much enhanced by magnetic fluctuations, the value of $(T_1T)^{-1}_{H_0\|a}$ corresponding to $N(E_F)$ is uncertain. However, if the $\boldsymbol{q}$ dependence of the HF coupling constants can be neglected, the rather small values of $(T_1T)^{-1}_{H_0\|a}$ in the AF state compared with $(T_1T)^{-1}_{H_0\|c}$ in the FIF state may correspond to a reduction of $N(E_F)$ through renormalization of Fermi surfaces.

We have also observed a stepwise enhancement of $(T_1T)^{-1}_{H_0\|c}$ above the metamagnetic transition at H_m, as shown

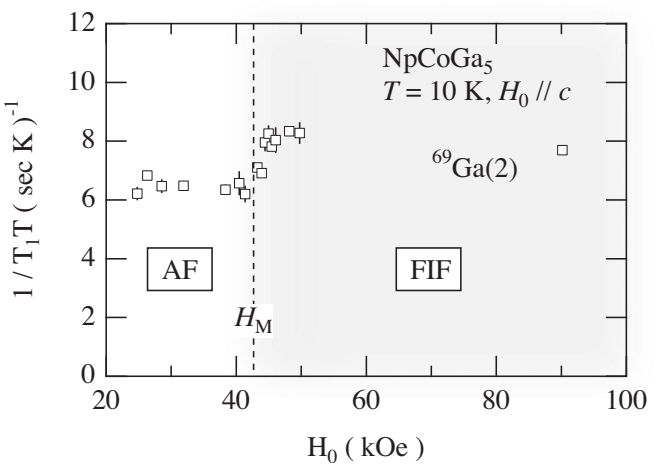

FIG. 18. The applied field dependence of $1/T_1T$ for ^{69}Ga(2).

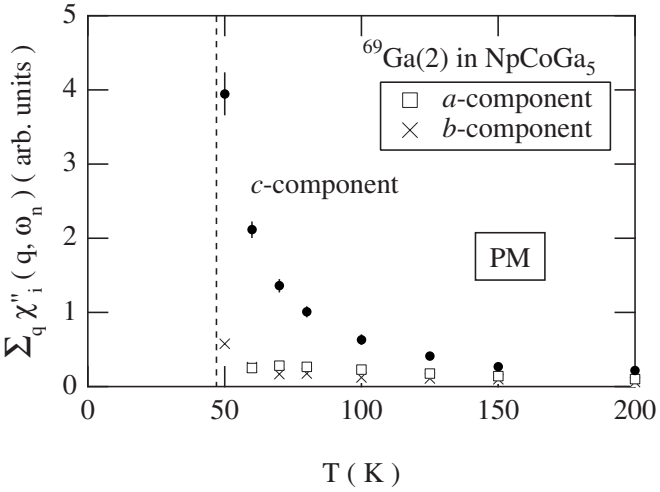

FIG. 19. The deduced $\boldsymbol{q}$-summed dynamical susceptibility in the PM state along the a, b, and c axes from spin-lattice relaxation rates for ^{69}Ga(2) (see text).

in Fig. 18. This increase in $(T_1T)^{-1}$ is thought to correspond to the modification of Fermi surfaces from AF to FIF phases, which has been observed in dHvA experiments.[35] Moreover, the lack of critical divergence at H_m in Fig. 18 suggests that AF to FIF is a first-order transition, which is consistent with neutron diffraction measurements.[34]

Lastly, let us discuss the anisotropy of spin fluctuations in the PM region as follows.[50] The spin-lattice relaxation measured with $H_0 \| c$ may be expressed[50]

$$(1/T_1T)_{H_0\|c} \propto \sum_{\boldsymbol{q}} [|A_a(\boldsymbol{q})|^2 \chi''_a(\boldsymbol{q},\omega_n) + |A_b(\boldsymbol{q})|^2 \chi''_b(\boldsymbol{q},\omega_n)], \tag{4}$$

where $A_i(\boldsymbol{q})$ is the $\boldsymbol{q}$ dependent HF coupling constant along the i axis. The subscripts in Eq. (4) can be permuted for other field directions.

We may represent $|A_i(\boldsymbol{q})|^2 = |A_i(0)|^2 f(\boldsymbol{q})$, where $f(\boldsymbol{q})$ is the HF form factor for that particular site. Since for Ga(2) the site symmetry is lower and HF fluctuations do not vanish with any particular field orientation, we make the simple approximation of neglecting the $\boldsymbol{q}$ dependence of $f(\boldsymbol{q})$. The $\boldsymbol{q}$ sums from Eq. (4) can then be written as $\Sigma_{\boldsymbol{q}} \chi''_i(\boldsymbol{q},\omega_n) \propto |A_i(0)|^{-2} \Sigma_j (1/T_1T)_{H_0\|j\neq i}$ for the Ga(2) site. Figure 19 shows the behavior of the $\Sigma_{\boldsymbol{q}} \chi''_i(\boldsymbol{q},\omega_n)$ deduced in this way. As temperature decreases toward T_N in the PM state, the c component of spin fluctuations becomes strongly predominant relative to the in-plane fluctuations below 100 K. The results shown in Fig. 19 closely mirror the behavior of the uniform susceptibility in this region.

2. T_2 measurements

In order to investigate the dynamical susceptibility anisotropy suggested in Fig. 19, measurements of the nuclear spin-spin relaxation time T_2 have been done with $H_0 \| a,c$. T_2 has been measured for ^{69}Ga(1), ^{69}Ga(2), and ^{59}Co (not shown). All T_2 values are obtained from single-exponential fits to spin-echo decay data. We also note that T_2 values for the center and satellite lines of the nuclei measured are nearly equal; i.e., T_2 has very little field dependence.

As shown in Fig. 20, the measured rates $1/T_2$ are larger than the corresponding $1/T_1$ values, corresponding to the expected dynamical susceptibility anisotropy. For the case of $H_0 \| c$, a sharp peak in $1/T_2$ is observed at T_N, whereas such a feature is not seen in the $1/T_1$ data. Since we measured $1/T_2$ for ^{69}Ga(2) at several field values, we also conclude that the peak position does not vary with external field. T_2 data for Ga(1) show markedly shorter values than for the Ga(2), partially accounting for the generally weaker Ga(1) signals. This effect evidently corresponds to larger transferred HF fields than for the Ga(2). Interestingly, the Ga(1) T_2 decay also appears to be peaking at T_N; thus, the strength of this decay shows that there are no AF correlations at high c axis field values.

To discuss the c axis T_2 results, we recall the equation for T_2 decay corresponding to Eq. (4), namely,[50]

$$\left(\frac{1}{T_2}\right)_c \simeq \frac{1}{2}\left(\frac{1}{T_1}\right)_c + \gamma_N^2 k_B T \lim_{\omega_n \to 0} \sum_{\boldsymbol{q}} |A_c(\boldsymbol{q})|^2 \frac{\chi''_c(\boldsymbol{q},\omega_n)}{\omega_n}. \tag{5}$$

The second term on the right simply refers to the divergent c axis fluctuations shown in Fig. 19, so that the T_2 peak in Fig. 20 (top) is presaged by the latter result. The participation of Ga(1) in this effect suggests that the fluctuations in this peak are not antiferromagnetically correlated. This is most remarkable, since the peak occurs exactly at T_N.

Finally, we note that there are now three effects which define the crossover point between the PM and FIF phases in the H-T phase diagram, i.e., the dotted line in Fig. 3. Originally defined by magnetization measurements as an inflection point, it was reaffirmed by sudden jumps in EFG components (Fig. 15) at the same temperature. It is also clear now from T_2 measurements at several field values that their fluctuation peak is also located at T_N, even at fields of ~100 kOe or whichever phase, PM or AF, is found on the low temperature side.

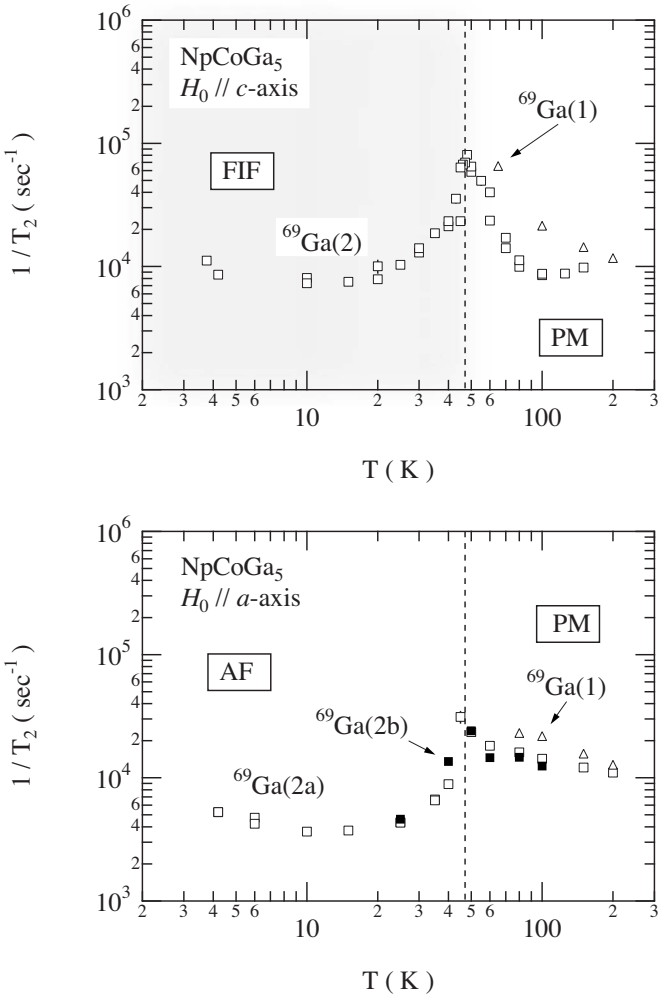

FIG. 20. Temperature dependence of spin-spin relaxation rates for ^{69}Ga(1) and ^{69}Ga(2). The upper panel shows the case of $H_0 \| c$ and the bottom shows $H_0 \| a$. The data for ^{69}Ga(2) in the case of $H_0 \| c$ taken under several applied fields of ~110 kOe (above H_m) are plotted together.

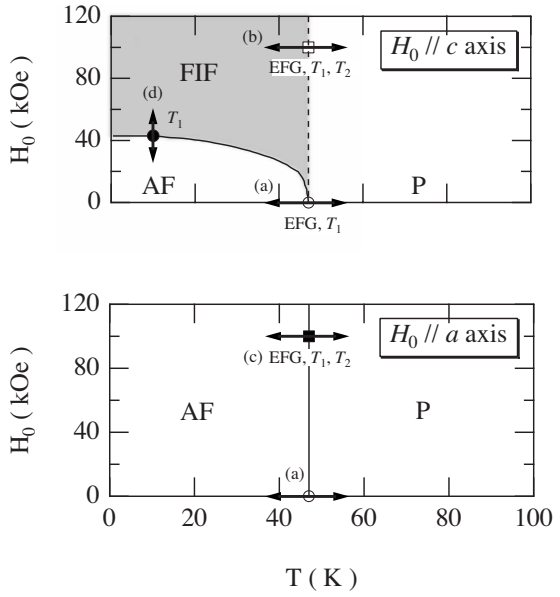

FIG. 21. Schematic diagram for the summary of these experiments. The thick-line arrows represent (a) T-scanned NQR experiment, [(b) and (c)] T-scanned NMR experiment with applied field along the c and a axes, respectively, and (d) H_0-scanned T_1 measurement.

IV. SUMMARY

We have performed a series of NMR/NQR experiments using a single crystal of itinerant antiferromagnet $NpCoGa_5$. The schematic H-T phase diagram is shown again in Fig. 21 in order to summarize our experimental results. Field-sweep NMR spectra have been recorded at fields above the metamagnetic (~40 kOe) transition, and the observed lines have been assigned to ^{69,71}Ga(1), ^{69,71}Ga(2), and ^{59}Co nuclear spins in the crystal. Using second-order perturbation theory to interpret quadrupole effects, Knight shift tensors and nuclear quadrupolar parameters (ν_Q and η) have been deduced from NMR data for the various sites over a wide range of temperatures, as shown by arrows (b) and (c) in Fig. 21. The quadrupolar parameters for the ^{69}Ga(1), ^{69}Ga(2), and ^{71}Ga(2) have been confirmed by NQR measurements using a single crystal in zero field, as shown by arrow (a) in Fig. 21. The nuclear quadrupolar parameters are found in zero field (AF state) to show temperature anomalies just below T_N, as shown by the open circle in Fig. 21.

Nuclear spin-lattice relaxation rates ($1/T_1$) for the nuclear sites suggest that the $5f$ electrons are very close to the localized limit at temperatures above ~100 K, but show itinerant behavior at temperatures between T_N=47 and 100 K. $1/T_1 \propto T$ behavior below ~100 K in the case of $H_0 \| c$ also indicates that the AF state in this material is characterized by itinerant $5f$ electrons. Moreover, orientation studies of $1/T_1$ have revealed a strong spin fluctuation anisotropy. We have observed a stepwise increase of $1/T_1$ at 10 K with applied field from AF to FIF states, as designated by arrow (d) and closed circle in Fig. 21. This increase in $1/T_1$ can be thought to correspond to a change in the density of states at the Fermi surfaces. A sharp peak in the measured nuclear spin-spin relaxation rates ($1/T_2$) clearly defines a crossover phase boundary between PM and FIF states located precisely at T_N, as denoted by the open square in Fig. 21. At this boundary of PM↔FIF, the observed anomaly of nuclear quadrupolar parameters is also found to coincide.

Even in $NpCoGa_5$, which is considered as a rather simple antiferromagnet compared with other Np115 systems, anomalies in the nuclear quadrupolar parameters have been observed just below T_N at the aforementioned crossover. As noted in theory papers[31,32] on Np115 systems, the $5f$ quadrupolar degree of freedom is quite important for understanding their peculiar phase transitions. To investigate the coupling between $5f$ charge states and nuclear quadrupoles in $NpCoGa_5$, further experimental results would be required, for example, the temperature variation of the lattice parameters or thermal expansion. Such a NMR/NQR study would establish a good foundation for investigation of other An115 compounds which exhibit complex magnetic and quadrupolar anomalies.

ACKNOWLEDGMENTS

We would like to thank T. D. Matsuda, Y. Haga, F. Honda, K. Kaneko, N. Metoki, T. Maehira, K. Kubo, H. Onishi, T. Hotta, E. Colineau, F. Wastin, and G. H. Lander for stimulating discussions and suggestions. We are also pleased to acknowledge the helpful suggestions of H. Harima. This research was partially supported by the Ministry of Education, Culture, Sports and Science and Technology, Grant-in-Aid for Young Scientists (B), 18740217, 2006.

*Present address: Physics Department, The University of Michigan, Ann Arbor, MI 48109, USA.

†Present address: DRFMC/SPSMS, CEA-Grenoble, Grenoble 38054, France.

[1] J. L. Sarrao, L. A. Morales, J. D. Thompson, B. L. Scott, G. R. Stewart, F. Wastin, J. Rebizant, P. Boulet, E. Colineau, and G. H. Lander, Nature (London) **420**, 297 (2002).

[2] F. Wastin, P. Boulet, J. Rebizant, E. Colineau, and G. H. Lander, J. Phys.: Condens. Matter **15**, S2279 (2003).

[3] C. Petrovic, P. G. Pagliuso, M. F. Hundley, R. Movshovich, J. L. Sarrao, J. D. Thompson, Z. Fisk, and P. Monthoux, J. Phys.: Condens. Matter **13**, L337 (2001).

[4] C. Petrovic, R. Movshovich, M. Jaime, P. G. Pagliuso, M. F. Hundley, J. L. Sarrao, Z. Fisk, and J. D. Thompson, Europhys. Lett. **53**, 354 (2001).

[5] R. Movshovich, M. Jaime, J. D. Thompson, C. Petrovic, Z. Fisk, P. G. Pagliuso, and J. L. Sarrao, Phys. Rev. Lett. **86**, 5152 (2001).

[6] H. Hegger, C. Petrovic, E. G. Moshopoulou, M. F. Hundley, J. L. Sarrao, Z. Fisk, and J. D. Thompson, Phys. Rev. Lett. **84**, 4986 (2000).

[7] G. F. Chen, K. Matsubayashi, S. Ban, K. Deguchi, and N. K. Sato, Phys. Rev. Lett. **97**, 017005 (2006).

[8] Y. Kohori, Y. Yamato, Y. Iwamoto, T. Kohara, E. D. Bauer, M. B. Maple, and J. L. Sarrao, Phys. Rev. B **64**, 134526 (2001).

[9] G.-q. Zheng, K. Tanabe, T. Mito, S. Kawasaki, Y. Kitaoka, D. Aoki, Y. Haga, and Y. Ōnuki, Phys. Rev. Lett. **86**, 4664 (2001).

[10] N. J. Curro, B. Simovic, P. C. Hammel, P. G. Pagliuso, J. L. Sarrao, J. D. Thompson, and G. B. Martins, Phys. Rev. B **64**, 180514(R) (2001).

[11] T. Mito, S. Kawasaki, G.-q. Zheng, Y. Kawasaki, K. Ishida, Y. Kitaoka, D. Aoki, Y. Haga, and Y. Ōnuki, Phys. Rev. B **63**, 220507(R) (2001).

[12] N. J. Curro, J. L. Sarrao, J. D. Thompson, P. G. Pagliuso, Š. Kos, A. Abanov, and D. Pines, Phys. Rev. Lett. **90**, 227202 (2003).

[13] S. Kawasaki, T. Mito, Y. Kawasaki, G.-q. Zheng, Y. Kitaoka, D. Aoki, Y. Haga, and Y. Ōnuki, Phys. Rev. Lett. **91**, 137001 (2003).

[14] S. Kawasaki, G.-q. Zheng, H. Kan, Y. Kitaoka, H. Shishido, and Y. Ōnuki, Phys. Rev. Lett. **94**, 037007 (2005).

[15] M. Yashima, S. Kawasaki, Y. Kawasaki, G. -q. Zheng, Y. Kitaoka, H. Shishido, R. Settai, Y. Haga, and Y. Ōnuki, J. Phys. Soc. Jpn. **73**, 2073 (2004).

[16] N. J. Curro, T. Caldwell, E. D. Bauer, L. A. Morales, M. J. Graf, Y. Bang, A. V. Balatsky, J. D. Thompson, and J. L. Sarrao, Nature (London) **434**, 622 (2005).

[17] H. Sakai, Y. Tokunaga, T. Fujimoto, S. Kambe, R. E. Walstedt, H. Yasuoka, D. Aoki, Y. Homma, E. Yamamoto, A. Nakamura, Y. Shiokawa, K. Nakajima, Y. Arai, T. D. Matsuda, Y. Haga, and Y. Ōnuki, J. Phys. Soc. Jpn. **74**, 1710 (2005).

[18] Y. Tokiwa, S. Ikeda, Y. Haga, T. Okubo, T. Iizuka, K. Sugiyama, A. Nakamura, and Y. Ōnuki, J. Phys. Soc. Jpn. **71**, 845 (2002).

[19] Y. Tokiwa, Y. Haga, N. Metoki, Y. Ishii, and Y. Ōnuki, J. Phys. Soc. Jpn. **71**, 725 (2002).

[20] Y. Tokiwa, T. Maehira, S. Ikeda, Y. Haga, E. Yamamoto, A. Nakamura, Y. Ōnuki, M. Higuchi, and A. Hasegawa, J. Phys. Soc. Jpn. **70**, 2982 (2001).

[21] S. Ikeda, Y. Tokiwa, T. Okubo, Y. Haga, E. Yamamoto, Y. Inada, R. Settai, and Y. Ōnuki, J. Nucl. Sci. Technol. **3**, 206 (2002).

[22] S. Ikeda, T. D. Matsuda, Y. Haga, E. Yamamoto, M. Nakashima, S. Kirita, T. C. Kobayashi, M. Hedo, Y. Uwatoko, H. Yamagami, H. Shishido, T. Ueda, R. Settai, and Y. Ōnuki, J. Phys. Soc. Jpn. **74**, 2277 (2005).

[23] S. Ikeda, Y. Tokiwa, T. D. Matsuda, A. Galatanu, E. Yamamoto, A. Nakamura, Y. Haga, and Y. Ōnuki, Physica B **359-361**, 1039 (2005).

[24] E. Colineau, P. Javorský, P. Boulet, F. Wastin, J. C. Griveau, J. Rebizant, J. P. Sanchez, and G. R. Stewart, Phys. Rev. B **69**, 184411 (2004).

[25] D. Aoki, Y. Homma, Y. Shiokawa, H. Sakai, E. Yamamoto, A. Nakamura, Y. Haga, R. Settai, and Y. Ōnuki, J. Phys. Soc. Jpn. **74**, 2323 (2005).

[26] F. Honda *et al.*, Physica B **359-361**, 1147 (2005).

[27] F. Honda, N. Metoki, K. Kaneko, S. Jonen, E. Yamamoto, D. Aoki, Y. Homma, Y. Shiokawa, and Y. Ōnuki, Physica B **378-380**, 1009 (2006).

[28] S. Jonen, N. Metoki, F. Honda, K. Kaneko, D. Aoki, Y. Homma, E. Yamamoto, Y. Haga, Y. Shiokawa, and Y. Ōnuki, Physica B **378-380**, 1018 (2006).

[29] F. Honda, N. Metoki, K. Kaneko, S. Jonen, E. Yamamoto, D. Aoki, Y. Homma, Y. Haga, Y. Shiokawa, and Y. Ōnuki, Phys. Rev. B **74**, 144413 (2006).

[30] S. Jonen, N. Metoki, F. Honda, K. Kaneko, E. Yamamoto, Y. Haga, D. Aoki, Y. Homma, Y. Shiokawa, and Y. Ōnuki, Phys. Rev. B **74**, 144412 (2006).

[31] H. Onishi and T. Hotta, New J. Phys. **6**, 193 (2004).

[32] A. Kiss and Y. Kuramoto, J. Phys. Soc. Jpn. **75**, 034709 (2006).

[33] D. Aoki, Y. Homma, Y. Shiokawa, E. Yamamoto, A. Nakamura, Y. Haga, R. Settai, T. Takeuchi, and Y. Ōnuki, J. Phys. Soc. Jpn. **73**, 1665 (2004).

[34] N. Metoki *et al.*, Phys. Rev. B **72**, 014460 (2005).

[35] D. Aoki, Y. Homma, Y. Shiokawa, E. Yamamoto, A. Nakamura, Y. Haga, R. Settai, and Y. Ōnuki, J. Phys. Soc. Jpn. **73**, 2608 (2004).

[36] T. Maehira, T. Hotta, K. Ueda, and A. Hasegawa, Phys. Rev. Lett. **90**, 207007 (2003).

[37] I. Opahle and P. M. Oppeneer, Phys. Rev. Lett. **90**, 157001 (2003).

[38] S. Ikeda, Y. Tokiwa, Y. Haga, E. Yamamoto, T. Ōkubo, M. Yamada, N. Nakamura, K. Sugiyama, K. Kindo, Y. Inada, H.

Yamagami, and Y. Ōnuki, J. Phys. Soc. Jpn. **72**, 576 (2003).
[39] G. H. Stauss, J. Chem. Phys. **40**, 1988 (1864).
[40] H. Kato, H. Sakai, Y. Tokiwa, S. Kambe, R. E. Walstedt, and Y. Ōnuki, J. Phys. Chem. Solids **63**, 1197 (2002).
[41] H. Kato, H. Sakai, Y. Tokunaga, Y. Tokiwa, S. Ikeda, Y. Ōnuki, S. Kambe, and R. E. Walstedt, J. Phys.: Condens. Matter **15**, S2001 (2003).
[42] H. Kato, H. Sakai, S. Kambe, R. E. Walstedt, Y. Tokiwa, and Y. Ōnuki, Acta Phys. Pol. B **34**, 1063 (2003).
[43] H. Kato, H. Sakai, Y. Tokunaga, Y. Tokiwa, S. Ikeda, Y. Ōnuki, S. Kambe, and R. E. Walstedt, J. Phys. Soc. Jpn. **72**, 2357 (2003).
[44] T. Ohama, H. Yasuoka, D. Mandrus, Z. Fisk, and J. Smith, J. Phys. Soc. Jpn. **64**, 2628 (1995).
[45] N. J. Curro, B. L. Young, J. Schmalian, and D. Pines, Phys. Rev. B **70**, 235117 (2004).
[46] A. A. Gusev, I. M. Reznik, and V. A. Tsitrin, J. Phys.: Condens. Matter **7**, 4855 (1995).
[47] R. M. Sternheimer, Phys. Rev. A **6**, 1702 (1972).
[48] S. Fraga, J. Karwowski, and K. M. S. Saxena, *Handbook of Atomic Data* (Elsevier Science, Amsterdam, 1976), p. 489.
[49] K. Kaneko, N. Metoki, N. Bernhoeft, G. H. Lander, Y. Ishii, S. Ikeda, Y. Tokiwa, Y. Haga, and Y. Ōnuki, Phys. Rev. B **68**, 214419 (2003).
[50] T. Moriya, Prog. Theor. Phys. **16**, 23641 (1956).
[51] T. Moriya and K. Ueda, Solid State Commun. **15**, 169 (1974).
[52] H. Sakai, S. Kambe, Y. Tokunaga, T. Fujimoto, R. E. Walstedt, H. Yasuoka, D. Aoki, Y. Homma, E. Yamamoto, A. Nakamura, Y. Shiokawa, K. Nakajima, Y. Arai, T. D. Matsuda, Y. Haga, and Y. Ōnuki, J. Magn. Magn. Mater. **310**, e118 (2007).